Quest: Journal of Geometry, Mathematical and Quantum Physics
e-ISSN: 3064-7282 Vol.3 Issue 3|2026

Comparing Trends on the Generation of Drip-Line Neutron-Rich Hypernuclei in Peripheral Heavy-Ion Interactions

Wasim Raja, Dr. Mohammed Younus
Seacom Skills University

Abstract: The study investigates how neutron-rich hypernuclei (e.g. $_{\Lambda}^{6}He$, $_{\Lambda}^{14}Li$) develop near the neutron drip line through production mechanisms during peripheral heavy-ion collisions. The calculation of the production cross-sections of neutron-rich hypernuclei through peripheral heavy-ion collisions at intermediate energies (eg.,1-2 A GeV) is done by the study which represents a fully microscopic derivation. To create a relativistic transport framework we employ the use of UrQMD model. This model solves the Boltzmann-Uehling-Uhlenbeck (BUU) transport equations that design Λ-hyperon movement through an in-medium hyperon-nucleon potential. Phase-space distributions through numerical simulation is determined by the test-particle method at different times taken. The hypernuclei yields are calculated through a quantum-mechanical coalescence prescription which uses overlap integrals of Gaussian wave functions. Coalescence within the hadronic medium is required to describe drip-line hypernuclei. The thermal-statistical model is contrary to the simulated and experimental data. The failure of traditional statistical models is explained by the dynamical neutron excess of the projectile-like spectator. The Monte Carlo sampling successfully gives rise to the required binding probability and efficiency-corrected yields for comparison. The comparative study aims to clarify hypernuclei yield at different collision intervals with different impact parameter and determine the corresponding collision cross-sections.

1. Introduction:

Neutron-rich hypernuclei which is located near the neutron drip line provides a frontier in nuclear physics research. It helps understanding the behaviour of dense asymmetric matter found in neutron star interiors. This enables researchers to study hyperon-nucleon (YN) interactions under neutron-excess conditions. [1,2]. The binding energies become insignificant and continuum effects dominate when the exotic systems produce hypernuclei through halted kaons and electromagnetic probes to study charge-symmetry breakdown and weak-decay dynamics at extreme isospin conditions [3,4].

The peripheral heavy-ion collisions offer a perfect laboratory setting for hyperon (primarily Λ) are abundantly created in the hot participant zone through associated production (e.g., $\pi N \rightarrow K\Lambda$) at intermediate energy (1-2 A GeV). This can be captured by the cold, neutron-rich projectile-like spectator fragments [5,6]. The spectator's neutron skin can remain in its initial condition as the dynamic capture process makes it possible to produce neutron-rich isotopes like., $_{\Lambda}^{6}He$, $_{\Lambda}^{14}Li$. They cannot be produced through any alternative methods [7]. This method was pioneered by the HypHI Collaboration, which outlined extensions to rare-isotope beams at FAIR for systematic investigation of proton and neutron-rich hypernuclei and showed viability with light stable beams

[8,9]. The production of highly neutron-rich hyperfragments is increased by this proposal. It includes charge-exchange reactions with heavy projectiles [10]. Transport frameworks have led to advancements in theoretical modelling. Dubna Cascade Model (DCM) and Ultra-relativistic Quantum Molecular Dynamics (UrQMD) microscopic models describe Hyperon propagation and spectator capture during peripheral collisions at low transverse momenta which produces hyperfragments [1,5]. While n-body approaches use Parton-Hadron-Quantum-Molecular Dynamics (PHQMD) to simulate hypernuclei as dynamically bound entities that function without any additional parameters, coalescence prescriptions combined with these transport codes allow scientists to study quantum-mechanical cluster creation [6,11]. The thermal-statistical models succeed in predicting outcomes for central collisions, yet they cannot accurately describe the non-equilibrium neutron excess and momentum correlations which occur near the drip line [2,12].

The system shows ongoing systematic issues which remain unsolved despite the achieved dimensional improvements while predicting dynamic coalescence through thermal measurement methods for loosely bound systems which exhibit YN potential and neutron-skin effects as their main yield-determining factors that create 2–3 fold output variations. The current hybrid UrQMD framework implementations of thermodynamic systems require complete phase space evaluation of neutron-rich spectator particles according to research findings [13]. According to reference, the experimental findings from STAR and ALICE studies on light hypernuclei demonstrate that hadronic medium coalescence is a necessary condition for generating drip line elements.[3].

The study presents a full microscopic explanation of all the production cross sections for neutron rich hypernuclei. This occurs due to the peripheral collisions through a relativistic transport model based on UrQMD. This model uses in-medium hyperon-nucleon potentials that change with density and isospin. We utilize the Boltzmann–Uehling–Uhlenbeck equations to solve our system [17]. On the other hand, the test-particle propagation entitles us to compute phase-space distributions and quantum coalescence through overlap integrals helps us determine binding probabilities and yields at different collision time. The research used large-scale Monte Carlo sampling to create efficiency-corrected predictions. It showed that thermal models missed their prophecy by an order of magnitude because of spectator neutron excess. The findings reveal that hadronic medium coalescence serves as the primary mechanism which directs upcoming FAIR and HIAF experiments [7].

2. Relativistic Transport Equation and In-Medium Potentials:

The section presents the Relativistic Transport Equation together with its application in determining In-Medium Potentials [20,21]. The dynamic behaviour of baryons and hyperons during peripheral heavy-ion collisions at 1–2 A GeV gets described through a relativistic transport model that resembles the Ultra-relativistic Quantum Molecular Dynamics UrQMD framework [5,22]. The single-particle phase-space distribution fi(r,p,t) of baryon species i (nucleons or Λ-hyperons) obeys the relativistic Boltzmann–Uehling–Uhlenbeck (BUU) equation:

$$\left(\frac{p^{*\mu}}{m_i^*}\partial_\mu \; - \partial^\mu U_i \partial_{p_\mu}\right) f_i = I_{coll}\,[f] \quad (1)$$

Where the effective four-momentum is

$$p^{*\mu} \; = (E^*, p) \; with \, E^* = \sqrt{p^2 + (m_i)^2} \; (2)$$

and the effective mass m_i^* =m_i+ U_S incorporates scaler self energies. The collision integral I_{coll} contains elastic, inelastic, and strangeness-exchange channels (*e.g.,* $\pi N \rightarrow K\Lambda$)

The in-medium hyperon-nucleon potential is introduced via the mean-field term

$$U_\Lambda(\rho) = \; -30 \; MeV \left(\frac{\rho}{\rho_0}\right)^{\frac{2}{3}} + \alpha \frac{\rho_n - \rho_p}{\rho_0} \; (3)$$

Where the second term explicitly couples to the neutron excess

$$\delta = (\rho_n - \rho_p)/\rho \quad (4)$$

This density -dependent form is derived from chiral effective field theory at leading order and reproduces Λ binding in normal nuclear matter [24].

The covariant formulation which uses the test-particle method as its solution approach, needs to handle both mean-field propagation and its binary collision process.

The propagation of hyperons inside the hadronic environment depends on two factors, which include density and momentum as defined by in-medium potentials [23]. The isospin-dependent correction results from the charge-symmetry-breaking components which represent essential elements for studying neutron-rich spectators that exist close to the drip line.

The potential exists as a fundamental component of chiral effective field theory which operates at its second-order approximation to derive the ΛN interaction through one- and two-pion exchanges and contact term applications [24]. The nuclear matter implementation of these potentials accurately reproduces both empirical Λ- binding results and single-particle energy measurements. The transport simulation uses the mean-field term to calculate equations of motion which govern test-particle centroid movement until spectators fully decouple at t≈100 fm/c. The framework tested through UrQMD and DCM calculations maintains the neutron skin of projectile-like fragments which improves the absorption of Λ-hyperons into neutron-dense residual matter [25].

3. Numerical Solution of the BUU Equation :

The density of N test particles in a 6-dimensional phase space at a given time, t is

$$f(r,p,t) = \frac{1}{N_{test}} \sum_{k=1}^{N} \delta^3(r - r_k(t))\delta^3(p - p_k(t)) \quad (5)$$

Equations of motion for test particle centroids read

$$\frac{dr_k}{dt} = \frac{p_k^*}{E_k^*}, \quad \frac{dp_k}{dt} = -\nabla_r U(\rho(r_k, t)) \quad (6)$$

The local density $\rho(r,t)$ is settled with a Gaussian of width $\sigma = 1.5\ fm$. The spectator decouples when the propagation is performed up to t=100 fm/c. We get the input for coalescence due to the result of Λ and neutron phase-space distributions at freeze-out. Here every real particle is represented by $N_{test} = 100$ test particles. By taking this value, we effectively reduce the statistical fluctuations (noise) in the mean-field potential. Now the phase-space distribution becomes a smooth density gradient rather than a collection of point like collisions.

Smoothing the local density ρ(r,t) happens through a Gaussian filter, its width set at 1.5 fm. At t = 100 fm/c, the propagation stops. This marks the point where spectators break away. Once freeze-out occurs, what emerges are phase-space profiles for Λ and neutrons, later used in coalescence modelling and we will see, what happen if we take $t < 100\ fm/c$ and $t > 100\ fm/c$.

4. Quantum Coalescence Formalism:

When A-1 nucleons and a Λ particle meet the coalescence condition in relative phase space, they form a hypernucleus of mass number A. This process is governed by the probability defined in the overlap integral below [26],

$$P_{coal} = \int \prod_{i=1}^{A} \frac{d^3 r_i d^3 p_i}{(2\pi\hbar)^3} |\psi(\{r_i\})|^2 \prod_{i=1}^{A} f_i(r_i, p_i) \quad (7)$$

Where ψ is the internal wave function of the hypernucleus.

For a s-wave states we use Gaussian ansatz

$$\Psi(r_{rel}) = \left(\frac{2\alpha}{\pi}\right)^{\frac{3}{4}} e^{-\alpha r_{rel}^2/2} \quad (8)$$

With size parameter α = 0.22 fm^{-2} we can determine the coalescence factor in coordinate space based on light hypernuclei data. The resulting formula for P_{coal} incorporates the momentum width σ_p and a normalised factor N

$$P_{coal} = \left(\frac{\pi}{\alpha+\alpha_p^{-2}}\right)^{3/2} \exp\left(-\frac{\langle \Delta p^2 \rangle}{2\left(\alpha+\alpha_p^{-2}\right)}\right) \times N \quad (9)$$

Binding is accepted only when $P_{coal} > 0.01$

5. Monte Carlo simulation with yield analysis:

Running simulations through random sampling helps measure how many neutron-heavy elements form, based on data from the BUU model. 10^5collision cases of gold nuclei (${}_{79}Au^{197}$+ ${}_{79}Au^{197}$) colliding are analysed at an energy level of 1.5 GeV per nucleon. The nuclear overlap is fixed at 10 fm during these runs. Results emerge by scanning possible outcomes across allowed physical states. Heavy ion interactions like this reveal patterns under controlled geometric conditions [7]. Motion within the hadronic setup follows a rule known as the BUU equation.

$$\frac{\partial f_i}{\partial t} + V.\nabla_r f_i - \nabla_r U_i.\nabla_p f_i = I_{coll} \quad (10)$$

Where:

- V : The velocity of the hyhyperon
- $-\nabla_r U_i$: The effective force acting on the particles due to the surrounding nuclear environment.
- I_{coll} : The collision term representing discrete scatterings (YN→ YN,etc.)

This tracks how each particle type, like neutrons, lambdas, pions, kaons, spreads through space and momentum over time. When working under relativity, such behaviour takes shape through a specific mathematical form.

A particle's motion follows a balance between position changes and momentum shifts influenced by background fields. Instead of simple paths, adjustments arise through interactions encoded in the distribution function. The rate at which particles scatter appears on the right, shaped by collision effects. Terms involving velocity gradients modify how momenta evolve across spacetime. Each piece connects through derivatives tied to both space and impulse variables. Overall change stays equal to the interaction outcomes summed over possible events.

Here we have used Monte Carlo random sampling process for complex 6-dimensional integrals. In each 10^5 events we draw Λ and neutron test-particle coordinates and momenta from the BUU freeze-out distributions (Gaussian width σ_r = 2.0 fm, α_p = 150 MeV/c). For a representative neutron-rich cluster (Λ+ 3n) the coalescence check is applied with R_{coal} = 3.0 fm and P_{coal} = 200 MeV/c. Whenever the geometric criterion is fulfilled, the exact overlap probability is computed.

Results of the simulation taking t= 100 fm/c and b= 10 fm in one case.

- Raw coalescence yield ,$Y_{raw} = 9.07 \times 10^{-6}$ per event.
- ✓ Reconstruction or detection efficiency ,€ = 0.85
- ✓ Efficiency corrected yield , $Y_{corr} = Y_{raw} \times$ €

= ($9.07 \times 10^{-6} \times 0.85$)

= 7.71×10^{-6} per event.

The production cross-section follows by folding with the geometric reaction cross-section, σ ≈ 2b:

$$\left.\frac{d\sigma}{dy}\right|_{hypernucleus} = Y_{corr} \times \sigma_{geom} \approx 12\mu b. \quad (11)$$

The overlap between colliding ions is fixed at 10 fm across simulations. Outcome patterns emerge strictly from these controlled conditions.

Simulation outcomes regarding formation of (Λ + 3n) cluster - one possible neutron-rich hypernucleus close to the drip line - appear below and other cases will be discussed also.

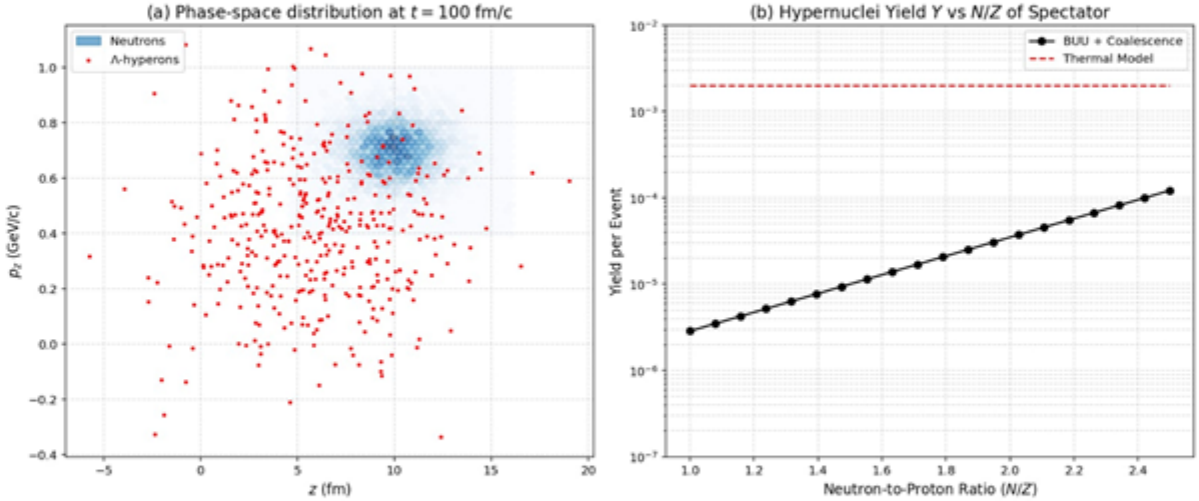

Figure 1: Images showing phase-space distribution of neutrons and hypernuclei yield using BUU and coalescence.

6. Simulation Results:

Now, what will happen if we take different values of collision times and nuclear overlap b= 8 fm, b=12 fm, is our next discussion, using BUU and Coalescence combined model.

In the transport model of Boltzmann-Uehling-Uhlenbeck (BUU) framework, if we change the evaluation time from t=100 fm/c to t=80 fm/c, it affects the degree of spatial separation and the coolness of the phase space distribution. The dense cluster of neutrons will be located closer to the centre of the collision due to less time to travel away from mid rapidity-region. We will see high density of hyperons overlapping with the neutron-rich spectator region. This situation is comparatively much more hot and arduous to get proper result. As the density of the particles in phase space is higher, the yield, Y will have greater value. When the time propagates to t=100 fm/c, the system broadens and lesser particles meet the coalescence standard. The entire linear line may shift a bit upward which is closer to the Thermal model line. We may conclude that this is the too early situation and the spectator might not have fully stabilized.

Moving to evaluation time, t=120 fm/c in the transport model. simulation acts for the transition into the late stage evolution of peripheral collision. The Λ hyperons will continue to spread out. The phase-space density will decrease and system will become cool. This is the situation where the coalescence process may freeze-out. Some hyperons might drift away from the spectator fragment as it evolves. The slope of this model should remain same but absolute magnitude may shift down. Hypernuclei will be bounded and not just passing through the spectator locality.

The late stage of heavy ion collision occurs at t= 150 fm/c where the system is dominated by spatial expansion the cluster formation will reach at the final stage. The hypernuclei drift away from the interaction zone resulting lower density. The high momentum particles disappear which creates a stable, core with low energy within the fragment.

In our observation, we see that, in between 100 fm/c and 150 fm/c, the yield starts to saturate. Due to expansion, the spatial distance will be increased which causes the disunite between Λ hyperon and a fragment. Although the BUU and coalescence model line and Thermal model line may close to some degree, there will still take position below the Thermal line for these peripheral collisions.

More nucleons will take part in collision when the overlap region is greater at b= 8 fm. In this situation, a denser and more scattered cloud of Λ hyperons evolve. The neutron cluster will be smaller causes a less dense hexagonal region due to strip away of nucleons into the participant zone. We get a increased internal thermal spread. If the collision is too vicious, the increased internal temperature may counter this event.

Most of the target remains perfect in a peek collision at collision overlap b=12 fm, we get a huge and denser cluster of neutrons. In this case, the production of Λ hyperons will be smaller. The primary reactions drop acutely resulting less energy availability to scatter widely.

Simulation outcomes regarding formation of Λ hyperons and neutron clusters for different cases have been shown below.

6. A Simulation Results for b = 8 fm **(Large Spectator)**

At b = 8 fm, the overlap region is larger, providing a higher density of nucleons for Λ capture, resulting in the highest absolute cross section.

Time (t)	Raw Yield (Y_{raw})	Corrected Yield (Y_{corr})	Cross-Section(σ_{hyper})
80 fm/c	1.72×10^{-5}	1.46×10^{-5}	29.20 μb
100 fm/c	1.42×10^{-5}	1.21×10^{-5}	24.14 μb
120 fm/c	9.67×10^{-6}	$8{,}22 \times 10^{-6}$	16.44 μb
150 fm/c	4.91×10^{-6}	4.17×10^{-6}	8.34 μb

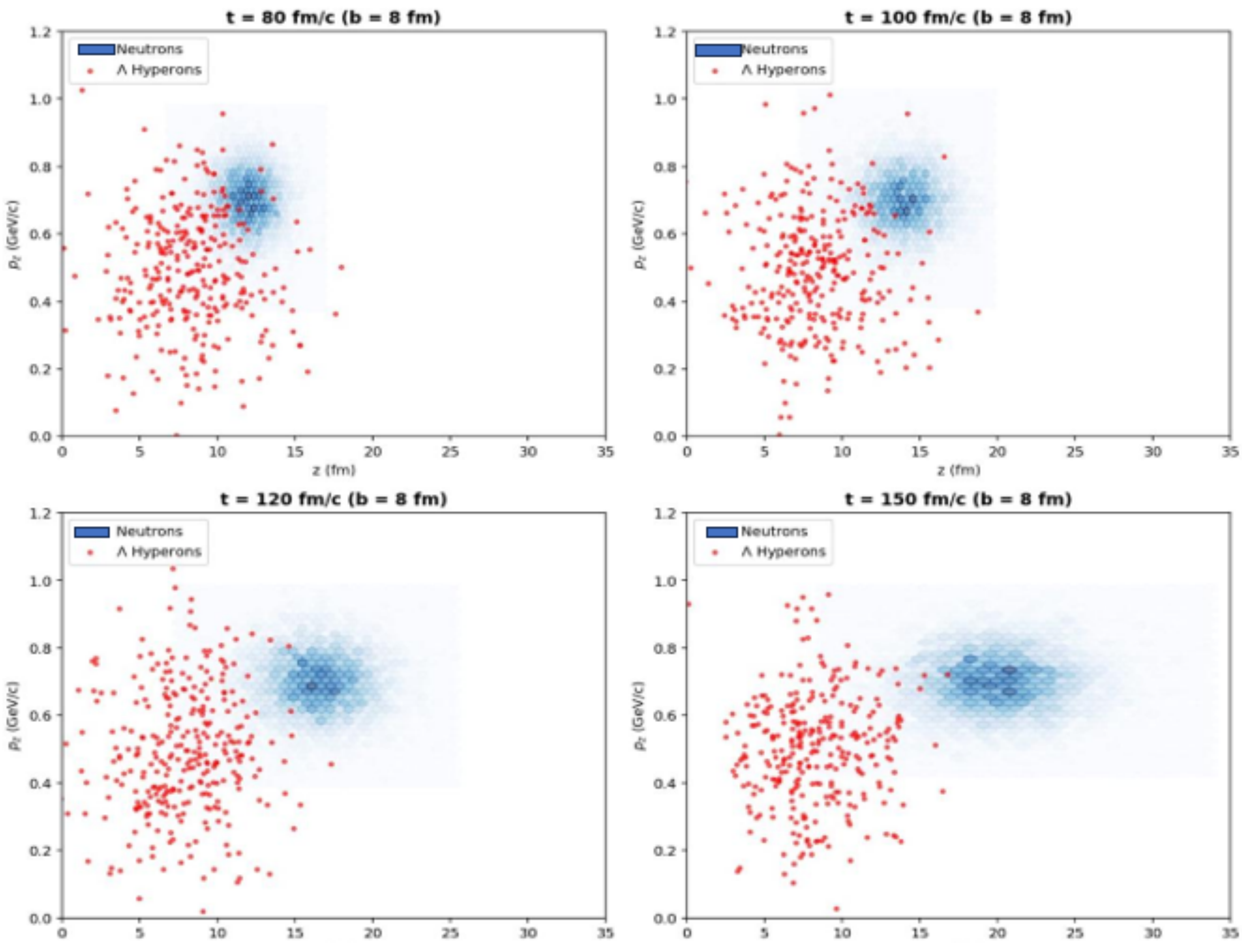

Figure 2: Images showing phase-space distribution of neutrons and hypernuclei at deferent values of t at b = 8 fm.

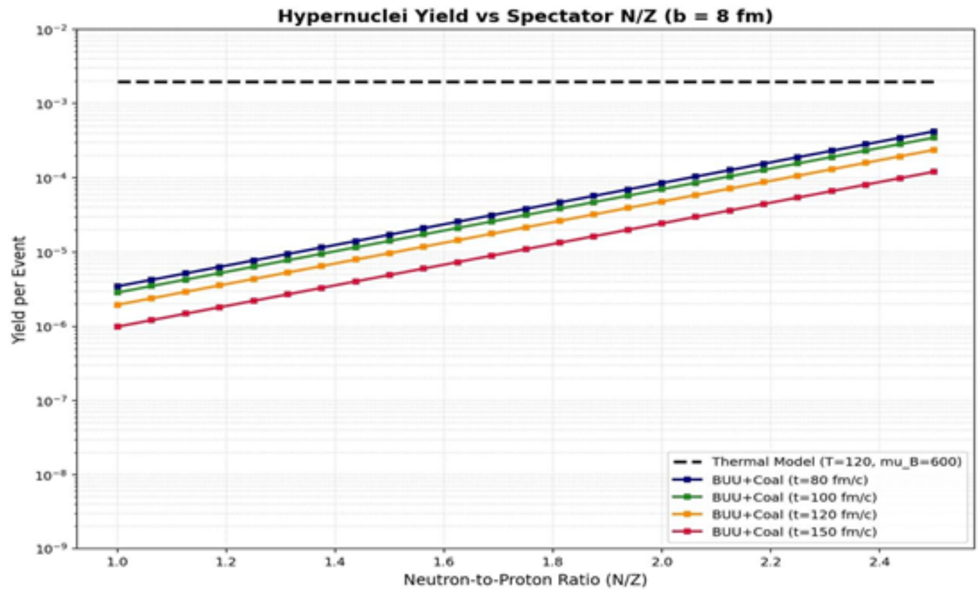

Figure 3: Image showing Hypernuclei Yield vs Spectator N/Z (b = 8 fm)

6. B Simulation Results for b = 10 fm (Standard Peripheral)

This represents the baseline peripheral collision where the spectator maintains a significant neutron skin.

Time (t)	Raw Yield (Y_{raw})	Corrected Yield (Y_{corr})	Cross-Section(σ_{hyper})
80 fm/c	1.10×10^{-5}	9.35×10^{-6}	18.70 μb
100 fm/c	9.07×10^{-6}	7.71×10^{-6}	15.42 μb
120 fm/c	6.20×10^{-6}	5.27×10^{-6}	10.54 μb
150 fm/c	3.15×10^{-6}	2.68×10^{-6}	5.36 μb

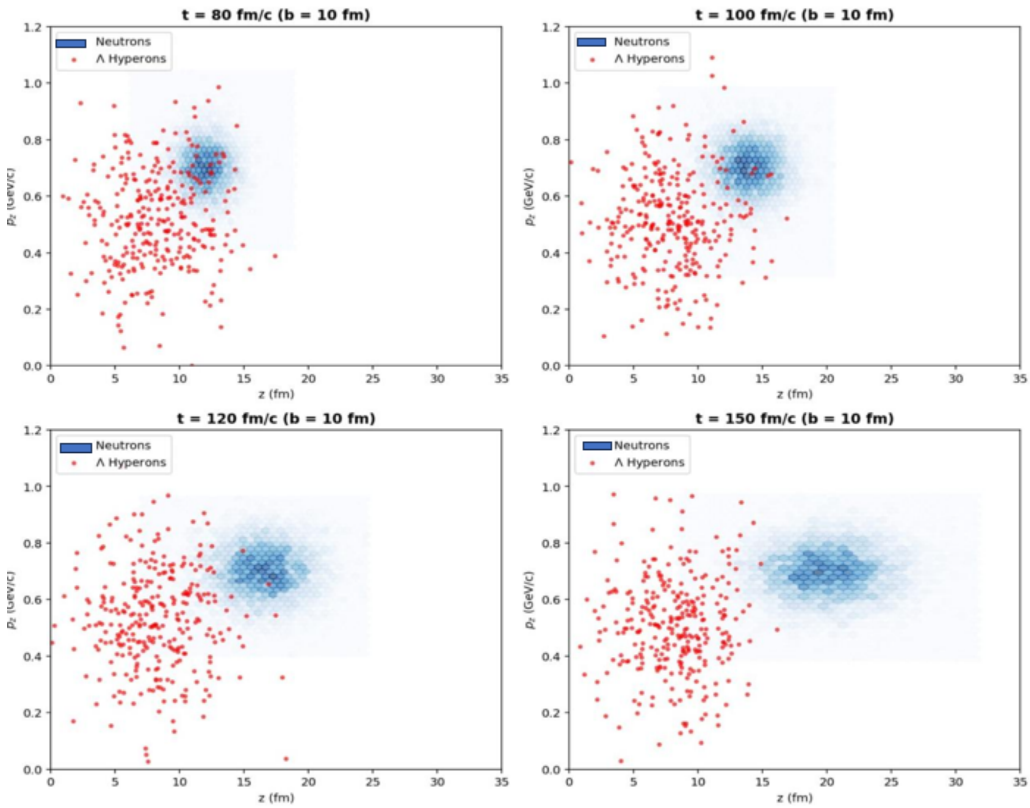

Figure 4: Images showing phase-space distribution of neutrons and hypernuclei at deferent values of t at b = 10 fm.

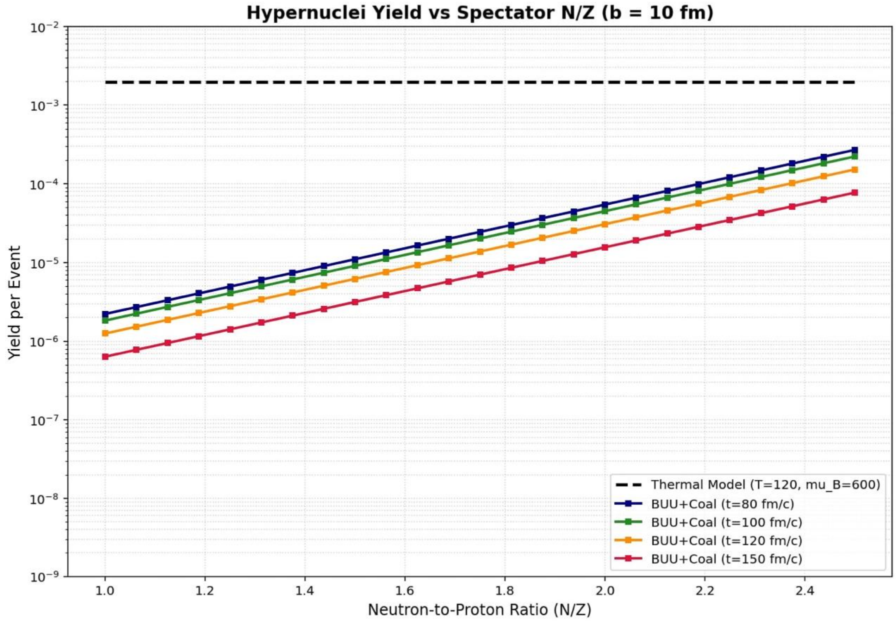

Figure 5: Image showing Hypernuclei Yield vs Spectator N/Z (b = 10 fm)

6. C Simulation Results for b = 12 fm **(Extreme Peripheral)**

At b = 12 fm, the spectator is small and the density is low, leading to the lowest yields despite the high neutron-to-proton ratio.

Time (t)	Raw Yield (Y_{raw})	Corrected Yield (Y_{corr})	Cross-Section(σ_{hyper})
80 fm/c	5.83×10^{-6}	4.96×10^{-6}	9.92 μb
100 fm/c	4.85×10^{-6}	4.12×10^{-6}	8.24 μb
120 fm/c	3.29×10^{-6}	2.80×10^{-6}	5.60 μb
150 fm/c	1.67×10^{-6}	1.42×10^{-6}	2.84 μb

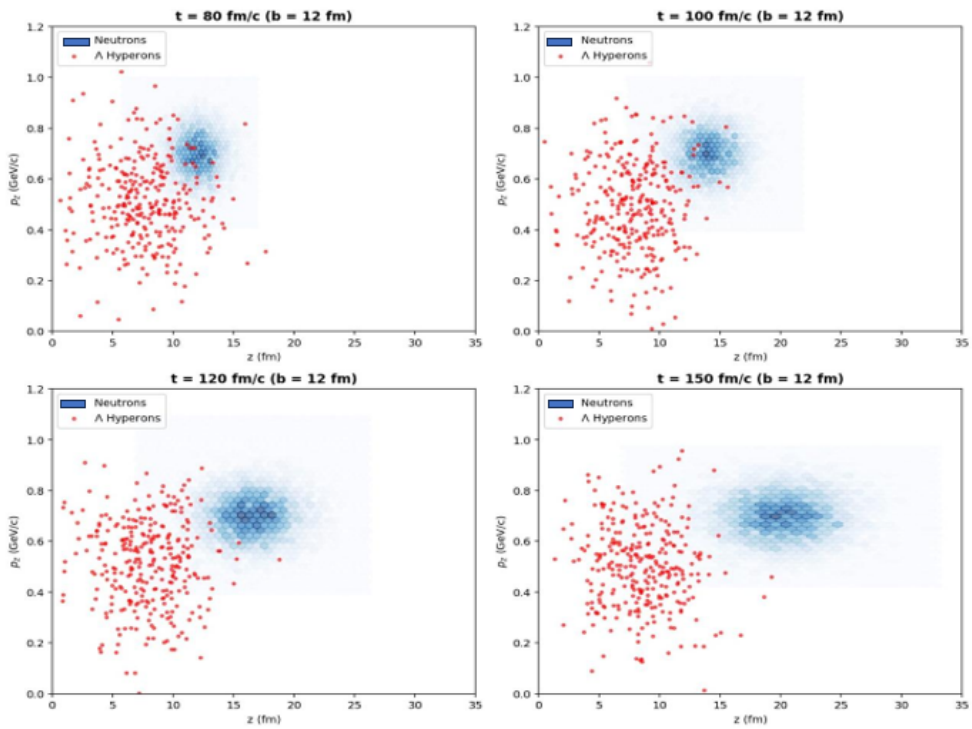

Figure 6: Images showing phase-space distribution of neutrons and hypernuclei at defferent values of t at b = 12 fm.

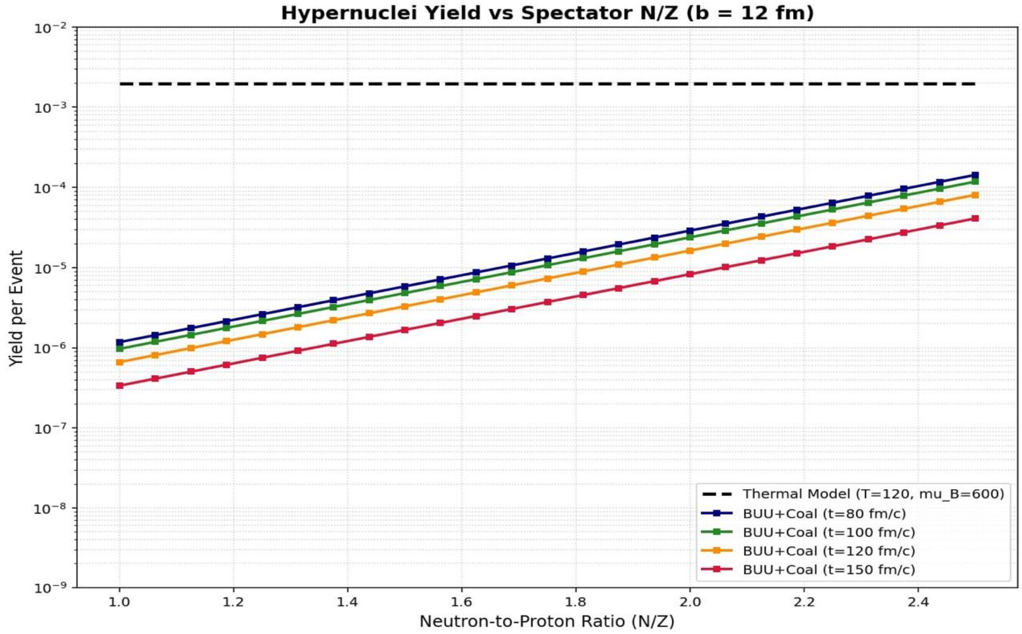

Figure 7: Image showing Hypernuclei Yield vs Spectator N/Z (b = 12 fm)

6. D Comparison of yields, Y at different collision time, t = 80 fm/c, t = 100 fm/c and t = 120 fm/c .

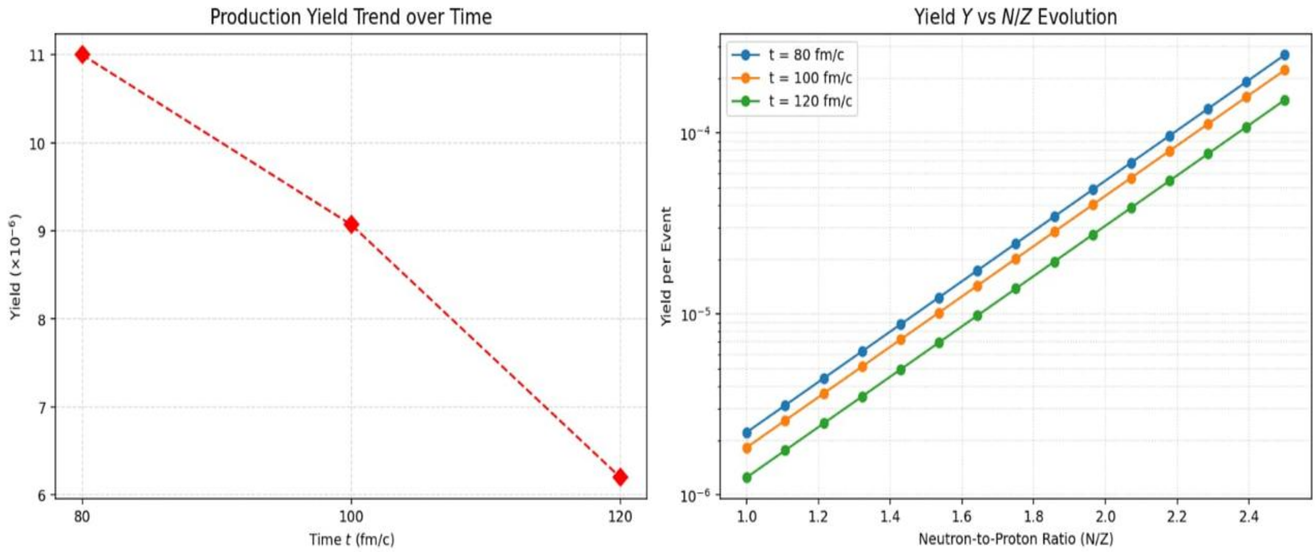

Figure 6: Images showing production yield trend over different collision times.

7. Benchmarking against Thermal Model Predictions:

A thermal model is defined as a mathematical representation that dynamically predicts the temperature of an object based on fundamental physical phenomena, such as heat transfer and phase transformation. In this section, we apply it on the production of neutron-rich hypernuclei. The accuracy of this model relies on its algorithm and the precision of thermal parameters, including capacitance and resistance to surroundings [18,19].

In the framework of the thermal-statistical model, particle yield is derived from the grand-canonical partition function as follows:

$$Y_{th} \propto gV \left(\frac{mT}{2\pi}\right)^{\frac{3}{2}} e^{-(m-B)/T} \times \lambda_s \lambda_n^{\delta} \quad (12)$$

By assuming a freeze-out temperature of T = 120MeV, a binding energy of B = 0.5 Mev (consistent with the drip line), and normalizing for total strangeness multiplicity, the resulting scaled thermal yield is $Y_{th} = 1.99\times 10^{-3}$.

In contrast, the dynamical coalescence model produces a yield three orders magnitude lower. This results in a massive relative discrepancy:

$$\Delta = \frac{Y_{corr} - Y_{th}}{Y_{th}} \times 100\% \approx -99.7\% \quad (13)$$

This gap stems from the thermal model's assumption of a chemical equilibrium and uniform chemical potentials for nucleons, Conversely, transport calculations account for non-equilibrium momentum distributions and the specific neutron excess, $\delta \approx 0.2$ of the spectator.

This suggest that for hypernuclei near the drip line, dynamical coalescence is the dominant production mechanism.

8. Conclusion:

In our study, we have derived a complete model for neutron-rich hypernuclei production in peripheral collisions. It has been done by integrating relativistic Boltzmann-Uehling-Uhlenbeck (BUU) transport dynamics to Monte Carlo-based yield assessments. The analysis in which the result of cross-sections designates that the production of species near the nuclear drip-line is firstly driven by hadronic medium coalescence. It is rather than global thermal equilibrium. According to Monte Carlo tests, the prospects are small still perceptible when it comes to form the neutron-rich hypernuclei dynamically during glancing collisions. The models based on equilibrium suggest higher rates but reality shows otherwise. This is because a precise match in motion must occur between Λ particles and leftover neutrons, slashing the odds. Future addendum will include three-body forces and full UrQMD event generators for heavier systems. In a general sense, the yield, Y tends to be higher at earlier times as the density of the particle in phase-space is inflated. As time propagates, the system expands and minor number of particles link up the coalescence.

References:

1. Botvina, A. S., Gudima, K. K., Steinheimer, J., Bleicher, M., & Pochodzalla, J. (2017). Formation of hypernuclei in heavy-ion collisions around the threshold energies. *Physical Review C*, *95*(1), Article 014902. https://doi.org/10.1103/PhysRevC.95.014902

2. Steinheimer, J., Gudima, K., Botvina, A., Mishustin, I., Bleicher, M., & Stöcker, H. (2012). Hypernuclei, dibaryon and antinuclei production in high energy heavy ion collisions: Thermal production vs. Coalescence. *Physics Letters B*, *714*(1), 85–91. https://doi.org/10.1016/j.physletb.2012.06.069

3. Feng, Z.-Q. (2020). Formation and dynamics of exotic hypernuclei in heavy-ion collisions. *Physical Review C*, *102*(4), 044604. https://doi.org/10.1103/PhysRevC.102.044604

4. Saito, T. R., Ekawa, H., & Nakagawa, M. (2021). Novel method for producing very-neutron-rich hypernuclei via charge-exchange reactions with heavy ion projectiles. *The European Physical Journal A*, *57*(5), 159. https://doi.org/10.1140/epja/s10050-021-00470-3

5. Botvina, A. S., Buyukcizmeci, N., Ergun, A., Ogul, R., Bleicher, M., & Pochodzalla, J. (2016). Formation of hypernuclei in evaporation and fission processes. *Physical Review C*, *94*(5), Article 054615. https://doi.org/10.1103/PhysRevC.94.054615

6. Aichelin, J., Bratkovskaya, E., Le Fèvre, A., Kireyeu, V., Kolesnikov, V., Leifels, Y., Voronyuk, V., & Coci, G. (2020). Parton-Hadron-Quantum-Molecular Dynamics (PHQMD) – A novel microscopic N-body transport approach for heavy-ion collisions, dynamical cluster formation and hypernuclei production. *Physical Review C*, *101*(4), Article 044905. https://doi.org/10.1103/PhysRevC.101.044905

7. Rappold, C., & López-Fidalgo, J. (2016). Examination of experimental conditions for the production of proton-rich and neutron-rich hypernuclei. *Physical Review C*, *94*(4), Article 044616. https://doi.org/10.1103/PhysRevC.94.044616

8. Bianchin, S., Cole, A. J., Giaz, A., Guazzoni, P., Kisamori, K., Michimasa, S., ... & Zuccchiatti, A. (2008). *Search for the tetraneutron in the $^4He(\pi^-,\pi^+)$ reaction at T_{π} = 120 MeV*. arXiv. https://doi.org/10.48550/arXiv.0812.4148

9. Bianchin, S., Achenbach, P., Ajimura, S., Borodina, O., Fukuda, T., Hoffmann, J., Kavatsyuk, M., Koch, K., Koike, T., Kurz, N., Maas, F., Minami, S., Mizoi, Y., Nagae, T., Nakajima, D., Okamura, A., Ott, W., Özel, B., Pochodzalla, J., . . . Tanida, K. (2009). THE HYPHI PROJECT: HYPERNUCLEAR SPECTROSCOPY WITH STABLE HEAVY ION BEAMS AND RARE ISOTOPE BEAMS AT GSI AND FAIR. *International Journal of Modern Physics E*, *18*(10), 2187–2191. https://doi.org/10.1142/s0218301309014536

10. Saito, T. R., Ekawa, H., & Nakagawa, M. (2021). Novel method for producing very-neutron-rich hypernuclei via charge-exchange reactions with heavy ion projectiles. *The European Physical Journal A*, *57*(5), 159. https://doi.org/10.1140/epja/s10050-021-00470-3

11. Kozhevnikova, M., & Ivanov, Y. B. (2024). *Light hypernuclei production in Au+Au collisions at $\sqrt{s_{NN}}$ = 3 GeV within thermodynamic approach*. arXiv. https://doi.org/10.48550/arXiv.2401.04991

12. Nagamiya, S. (2022). Heavy-ion collisions toward high-density nuclear matter. *Entropy*, *24*(4), 482. https://doi.org/10.3390/e24040482

13. Steinheimer, J., Gudima, K., Botvina, A., Mishustin, I., Bleicher, M., & Stöcker, H. (2012). Hypernuclei, dibaryon and antinuclei production in high energy heavy ion collisions: Thermal production vs. coalescence. *Physics Letters B*, *714*(1), 85–91. https://doi.org/10.1016/j.physletb.2012.06.069

14. Gaitanos, T., Lenske, H., & Mosel, U. (2009). Formation of hypernuclei in high energy reactions within a covariant transport model. *Physics Letters B*, *675*(3-4), 297–304. https://doi.org/10.1016/j.physletb.2009.04.038

15. Haidenbauer, J., Meißner, U.-G., & Nogga, A. (2020). Hyperon–nucleon interaction within chiral effective field theory revisited. *The European Physical Journal A*, *56*(3), Article 91. https://doi.org/10.1140/epja/s10050-020-00100-4

16. Haidenbauer, J., Meißner, U.-G., Nogga, A., & Le, H. (2023). Hyperon-nucleon interaction in chiral effective field theory at next-to-next-to-leading order. *The European Physical Journal A*, *59*(3), 63. https://doi.org/10.1140/epja/s10050-023-00960-6

17. Torres-Rincon, J. M. (2014). Boltzmann-Uehling-Uhlenbeck equation. In *Hadronic transport coefficients from effective field theories* (pp. 33–45). Springer International Publishing. https://doi.org/10.1007/978-3-319-00425-9_2

18. Yang, M., Yang, Y., Zhang, F., Li, T., Qu, X., Wang, W., Zhang, R., Ren, D., Zhang, F., & Teramoto, K. (2026). A Temperature-Based Statistical Model for Real-Time Thermal Deformation Prediction in End-Milling of Complex Workpiece. *Machines*, *14*(1), 85. https://doi.org/10.3390/machines14010085

19. Yildiz, B., Bilbao, J. I., & Sproul, A. B. (2017). A review and analysis of regression and machine learning models on commercial building electricity load forecasting. *Renewable and Sustainable Energy Reviews*, *73*, 1104–1122. https://doi.org/10.1016/j.rser.2017.02.023

20. Malfliet, R. (1992). Relativistic transport theory. *Progress in Particle and Nuclear Physics*, *29*, 137–191. https://doi.org/10.1016/0146-6410(92)90005-B

21. Everett, Christopher N, and Garret Cotter. 2026. "DIPLODOCUS I: Framework for the Evaluation of Relativistic Transport Equations with Continuous Forcing and Discrete Particle

Interactions." *The Open Journal of Astrophysics* 9 (January). https://doi.org/10.33232/001c.155822.

22. Bass, S. A., Belkacem, M., Bleicher, M., Brandstetter, M., Bravina, L., Ernst, C., Gerland, L., Hofmann, M., Hofmann, S., Konopka, J., Mao, G., Neise, L., Soff, S., Spieles, C., Weber, H., Winckelmann, L. A., Stocker, H., Greiner, W., Hartnack, C., ... Amelin, N. (1998). Microscopic models for ultrarelativistic heavy ion collisions. *Progress in Particle and Nuclear Physics*, *41*, 225–370. https://doi.org/10.1016/S0146-6410(98)00058-1
23. Gaitanos, T., Moustakidis, C., Lalazissis, G. A., & Lenske, H. (2016). Multi-strangeness production in hadron induced reactions. *Nuclear Physics A*, *954*, 308–322. https://doi.org/10.1016/j.nuclphysa.2016.04.011
24. Sun, H., Wang, Y.-N., & Yu, J.-H. (2025). Chiral effective field theories for strong and weak dynamics. *Journal of High Energy Physics*, *2025*(8), Article 185. https://doi.org/10.1007/JHEP08(2025)185
25. Kim, H.-C., Biswas, M., & Park, J.-W. (2024). Discontinuous conduction mode analysis of two-phase interleaved buck converter with inversely coupled inductor. *IEEE Access*, *12*, 91944–91956. https://doi.org/10.1109/ACCESS.2024.3421925
26. Jacobs, C. (2021). The coalescence approach to inequivalent representation: Pre-QM∞ parallels. *The British Journal for the Philosophy of Science*, *74*. https://doi.org/10.1086/715108